Fungal pigments on paper: Raman and Quantum Chemistry studies of *Alternaria* Sp.

Victor V. Volkov and Carole C. Perry*

Interdisciplinary Biomedical Research Centre, School of Science and Technology, Nottingham Trent University, Clifton Lane, Nottingham NG11 8NS, United Kingdom.

ABSTRACT

To advance our understanding of the molecular biochemistry of fungi which impact cultural heritage in libraries, museums and archives we investigated the diagnostic capacity of Raman spectroscopy to identify the composition of colored chromophores of fungi on paper. In this study we explored the diagnostic capacity of resonant Raman to distinguish chromophores in fungal filaments stimulated to grow on paper under high humidity with a focus on characterizing chromophores of *Alternaria* group species. To facilitate molecular analysis, we conducted quantum chemistry calculations of representative metabolites having optical absorption in the ultraviolet-visible spectral range. Comparing theory and experiment we show that fonsecin, erythroglaucin and aurasperone type chromophores occur in mature hyphal filaments with β-carotene dominant in yeast depositions on paper surfaces. Resonant Raman of mature filaments suggests a further contribution of carotenes longer than β-carotene to the spectral signature. Using microscopic resolution, we distinguish rich sets of Raman signatures that we assign to lignin, flavoglaucin, riboflavin, cycloleucomelon(e) and asperyellone molecular components in the spatial regions where filaments initiate from yeast depositions. In such regions, where filament microstructures stimulate development of a mature three-dimensional scaffold, the diversity of Raman resonances confirms a rich biochemistry of the developing structures. The library of computed optical and spectroscopic responses of characteristic fungal chromophores and metabolites presented here is essential for understanding the effect of fungi on a wide range of objects made from paper including books, prints, drawings, watercolors, engravings and even sculptures as well as designing next generation materials based on fungal hyphal mats.

KEYWORDS Raman, Microscopy, Fungi, Paper, Optical, Density Functional Theory

INTRODUCTION

The early [1] specialization of the fungal kingdom was due to the conceptual way proto-fungal cells rely on the biology of a permeable wall to provide fast-molecular transport and to digest food externally. The latter plays a crucial role for fungi in our life: in industry and in culture. If the idea of systematic employment of fungi as productive agents developed slowly, since intuitive ancient fermentations, to express in design of the first pharma-chemical protocols of oxalic acid production at the end of XIX century [2], awareness of fungi as active participant in our daily life either as pathogens, or as symbionts, or as an indifferent-competitive living force started to take shape only within the last several decades, and only after understanding that these organisms form their own kingdom [3].

Fungi have a drastic impact on human culture and here we discuss heritage preserved in paper artefacts. Paper is a sheet material made of cellulose fibres. Within the last two millennia, paper was the main "support" of information storage and transfer in daily use, ousting wax and clay tablets, birch bark, and leather parchments. As a hygroscopic organic material, made of polysaccharide chains, paper may be a source of nourishment for many micro-organisms. Fungi are the main group to play a role in paper degradation [4]. They are the main threat to the written and printed heritage in libraries, archives, and museums [5]. Various *Aspergillus*, *Fusarium*, *Trichoderma*, *Myrothecium*, and *Penicillium* species demonstrate effective growth on paper and cause substrate chemical alterations upon

excretion of hydrolytic enzymes. [6]. Cellulases and various proteases are the main culprits [7]. Further, it has been shown that basidiomycetes are potent lignin decomposers [8]; *Trichosporon cutaneum*, *T. pullulans*, and *Cryptococcus* spp. are capable of digesting pectins using pectinase [9]; also, some strains of *T. cutaneum* and *T. pullulans* can convert xylans into xylose saccharides using xylanase [10]. Beside excretion of hydrolytic enzymes, fungal growth leads to deposition of organic and inorganic acids, lipids, chelating agents, calcium oxalate crystals, glycerine and other biochemical substances in paper [7]. All these components have different effects on the structural and electronic properties of paper at the site of deposition. Paper bio-deterioration is a complex mixture of physical and chemical processes. Several factors, such as the cellulose source, the manufacturing processes, contributions of lignin and metallic compounds, and environmental conditions play a role [11]. For example, since cellulose may be present either in crystalline or amorphous form, it has been reported that the latter is more susceptible to bio-deterioration [12]. Also, while removal of lignin in papermaking helps generate a better quality of paper, this weakens a paper's resistivity to fungal attack [13].

Typically, fungal growth on paper is associated with color changes at the site of growth. In the case of fast fungal growth, this is mainly because the fungal structures themselves are often coloured black, brown, red, yellow and purple [14,15]. The coloring of fungal cells is due to secondary metabolites [16] and these are the principle focus of this manuscript. Local changes of a paper's color (foxing) signify the presence of fungi in paper [17]. Recent studies ascribe such changes of color to interactions of fungal excretions with chemical components of the substrate (paper). As examples, autoxidation of released lipids may provide free-radicals and peroxides [14] giving rise to localized cellulose oxidation [18] that can be correlated with the heterogeneity of cellulose structure (crystalline versus amorphous) and humidity [19]. An alternative or competitive mechanism of long-term foxing may involve the effects of fungal activity products on metal ion inclusions in paper [17,20]. As an example, fungal production of acid can stimulate formation of organic ferrous salts that decompose (by oxidation) into iron oxide or hydroxide leading to a brown coloration [21,22].

To develop systematic diagnostics of fungal species at the molecular level we must distinguish different chromophores/pigments. Raman spectroscopy is a useful tool in this respect as the technique has a number of practical advantages: (1) it has sensitivity to detect responses from several molecules under light microscopic spatial resolution; (2) signals are characteristic of molecular structure; (3) it has an unprecedented specificity to excitation wavelength and to the polarization of light [23-25]; (4) Raman samples can be taken *in vivo* outside of a lab and sampling can be non-invasive; (5) Raman signals can be computed using Quantum Chemistry; (6) using results of Quantum Chemistry we may model orientational molecular distributions of chemical entities using observed Raman intensities when sampled at interfaces; and (7) sampling of Raman signals may be correlated with mass spectrometry and scanning electron microscopy [26]. The starting point in developing systematic Raman diagnostics is possible as signals are characteristic of molecular structure as in (2) above. Using chemical quantum theory we can develop a database of Raman tensors computed using certified theory levels for representative structures (and their variances) of molecular systems which may contribute to the detected spectral responses. To facilitate the approach, we use a systematic grouping of the representative molecular structures including the pteridines, the melanins; the quinones (anthra-, benzo-, terphenyl-), and the carotenes/ carotenoids [27].

Among the groups of chromophores, in recent studies, special attention has been given to characterization of the melanin pigments of *Aspergillus* hyphae over time. This is of a general value because the described biochemistry and spectra of intermediate metabolites are common for various genera of filamentous fungi. In an introduction to melanin biochemistry in *Aspergillus* [28] it was proposed that the pigment aspergillin (molecular weight of about 20000) is formed from two precursors. The first component consists of a "green" pigment hexahydroxyl pentacyclic quinoid (HPQ)

with optical absorption maximum at 575 nm; the second component consists of a “brown” melanin pigment with unknown molecular weight and optical absorption maximum at 425 nm. Recent progress in genetic engineering and the control of synthesis of melanin pigments in conidia [29] has suggested the presence of naphtho-pyrone, aurasperone, flavasperone, fonsecin and funalenone secondary metabolites all reported as coloring chromophores of various filamentous fungi growing on paper [30] and described by Wolf [27] as being present during the development of ‘melanin-like’ pigments [29].

Our research aim is to understand if there could be bio-molecular markers to reflect active fungal biology including various proliferation mechanisms [30], which impact cultural heritage in libraries, museums and archives [5,7,13-17,31]. In this contribution, we investigated the diagnostic capacity of Raman spectroscopy to identify the composition of colored chromophores in filaments of fast-growing fungi opportunistically stimulated on paper under high levels of humidity. Under these conditions, we observed competitive growth of *Alternaria*, *Chaetomium* and *Aspergillus* group species, which present brown/green/black coloring, and are the most typical genera reported to affect the preservation of paper [32]. Under growth conditions of high humidity and access to water, we observed dominance of *Alternaria* group species. Thus, the characterization of this group is the main focus of this investigation. At the same time, the approach may be extended to improve our knowledge on other species affecting paper and other substrates, as well.

The outline of the manuscript is as follows. First, we provide visual microscopy characterization of typical species stimulated to grow on paper. Second, we sample Raman signatures for microstructures of *Alternaria* group species, mainly. Third, with the results of previous studies [27,33] as a starting point we build a database of representative molecular structures for quantum chemistry studies, extract optical absorption properties in the ultraviolet-visible spectral range and compute Raman (resonant and non-resonant) responses. Finally, using the computed properties we review the experimental Raman data and discuss the practical implications of the approach. Here it is important to note that although we focus our analysis on *Alternaria* group species, the computed properties of the database of representative molecular structure should be valuable for discussion of the electronic and structural properties of molecular species in other filamentous fungal species that are known to grow on a wide range of materials and hence to affect books, prints, drawings, watercolors, engravings and even sculptures [5,7,13-17,31].

MATERIALS AND METHODS

Growth conditions

We explored fungal colonial growth under various levels of humidity (100, 90, 80 and 70%). To grow fungi, we used a standard office paper and a vintage paper. The office paper (80 g/m^2) was selected from a local provider requiring that it be produced under elemental chlorine free bleaching of wood pulp to demonstrate a lesser degree of whiteness (value 92 by Commission Internationale de l’Eclairage) in order to avoid possible complications due to optical brightening agents and other fillers. Specifically, we confirmed the lack of fluorescent agents using a black light source Convoy s2+ nichia flashlight with radiation at 365 nm (full width at half maximum). The vintage paper was produced in the XVIII century in a paper mill in the County of Kent, England. In Supplementary information **Fig. S1**, we show that the office paper contained a significantly smaller contribution of crystalline cellulose compared to the vintage paper [34]. As lower levels of cellulose crystallinity are beneficial for the rapid initial growth of fungi, and because the aim of our research was the characterization of chromophores specific to *Alternaria* sp., in this report we discuss experimental results for fungi cultures grown on the office paper.

The colonies were grown in a laboratory space under active thermoregulation set to confirm 22^{o}C, and with illuminance of about 20-50 lux. Imaging of cultures was accomplished using a Wild

stereomicroscope (Heerbrugg, Switzerland) equipped with a UCMOS14000KPA C-mount camera (Touptek, Hangzhou, P. R. China). To characterise optical absorption of pigments and chromophore methanol extracts in the ultraviolet-visible spectral range, we used an ATi Unicam UV/VIS spectrometer (Akribis Scientific Ltd).

Raman experiment

We conducted Raman spectral studies using a DXR microscope (Thermo Fisher Scientific, Madison, WI, United States) equipped with 50× and 100× objectives, a diode-pumped solid-state laser at 532 nm and a thermoelectrically cooled 324 FI CCD camera, Andor Technology Ltd. of Oxford Instruments. The spectral resolution in Raman experiments is 2 cm^{-1} according to the instrumental limit of the microscope operated with a 25 micron confocal pinhole. Spectral responses were stimulated using 2 mW of unpolarised radiation. Our studies of focusing may suggest that the spectral responses were collected from the area with diameter smaller than 600 nm. Since we used a specific wavelength to stimulate experimental Raman, we may expect pre-resonant effects due to the electronic transitions of various pigments in fungal cultures. Specifically, relative Raman intensities may change dramatically when we tune the wavelength of excitation to be close to the electronic transition of a specific chromophore [23-25]. To account for this in our discussion, we reviewed the electronic properties of chromophores, the main structural elements of which may be considered representative of what may be found in fungi.

Model molecular systems for theoretical studies

To develop a reference database of Raman responses, we selected a number of chromophores grouped according to a prior study [27], **Fig. 1.** The first group included chromophores having three rings condensed under nonlinear and linear arrangements with examples as alternariol, flavosperone, funalenone, and fonsecin, see **Fig. 1**. Alternariol is a benzochromenone pigment, $C_{14}H_{10}O_5$, 258.23 g/mol, [35], and is considered the most important mycotoxin produced by the black mould *Alternaria* species to grow on grain cereals worldwide. Flavosperone is a yellow benzochromene or naphthopyran, $C_{16}H_{14}O_4$, 270.28 g/mol, extracted from *Aspergillus* species [36]. Funalenone is a phenalene compound, $C_{15}H_{12}O_6$, 288.3 g/mol, isolated from *Aspergillus niger* [29,37]. Fonsecin, $C_{15}H_{14}O_6$, 290.27 g/mol, is naphtho-γ-pyrone metabolite typical for Aspergillus species [36].

The second group accounts quinones (diketones) including flavoglaucin, cycloleucomelon(e) and erythroglaucin, see **Fig. 1**. Flavoglaucin is a yellow pigment: it is among the simplest hydroquinones [27,38]: $C_{19}H_{28}O_3$, 304.4 g/mol. Originally, it was isolated from *Aspergillus glaucus* [38] and *Aspergillus echinulatus* [40]. The molecule is considered as a metabolite typical for this group of species. Cycloleucomelon(e), is a green pigment [41] originally described as benzoquinone, $C_{18}H_{10}O_7$, 338.268 g/mol, isolated from *Boletopsis leucomelaena*, *Tapinella atrotomentosa* and *Anthracophyllum* species [42] and as a secondary metabolite from *Aspergillus niger* [43]. Erythroglaucin, $C_{16}H_{12}O_6$, 300.26 g/mol, is an aromatic ether and a trihydroxyanthraquinone: it was reported to be present in *Aspergillus* and *Chaetomium* species as a metabolite [43,44].

The third group contains chromophores with higher structural complexity and includes naphthopyrones where two conjugated sets of aromatic cycles are connected with a single bond. Naphthopyrones are known for various bioactive properties [29,45]. In our studies we considered the slightly simplified molecules, aurasperone and Isonigerone, see **Fig. 1**. Aurasperone A is a dimeric naphthopyran with formula $C_{32}H_{26}O_{10}$, 570.5 g/mol, originally isolated from *Aspergillus niger* [35]. Isonigerone (of the same formula and molecular weight) belongs to the class of organic compounds known as naphthopyranones [46].

The fourth group of chromophores includes the pteridines. Specifically, riboflavin, more commonly known as vitamin B12, is a d-ribitol with a characteristic benzo-γ-pteridine structural motif in position

5, $C_{17}H_{20}N_4O_6$, 376.4 g/mol. The fifth group of chromophores includes those molecules that determine the black color of *Aspergillus niger* conidia [27]. Based on the results of previous theoretical studies [47], we choose eumelanin-melanin trimer and "green aspergilline" hexahydroxyl pentacyclic quinoid, $C_{19}H_{12}O_8$, [28,29] as examples. Finally, in the sixth group of chromophores, we include chromophores with π-electron conjugation with asperyellone [29] and beta-carotene [27] taken as examples. Beta-carotene has previously been detected in *Alternaria* species [35].

To anticipate possible spectral contributions of the structural component of the cell walls we calculated the properties of a simple glycopeptide and a lignin-like structural segment, with generic structures, as shown in **Fig. 1**. We developed the glycopeptide model accounting both, the results of recent coherent Raman studies in yeast cells and spores of *Schizosaccharomyces pombe* known to lack optical absorption in the visible [48], and structural properties of a glycopeptide by X-ray studies for *Pycnoporus coccineus* [49]. Since no aromatic side-groups are included in the structure, we disregard the resonance contribution of UV electronic transitions of the polypeptide backbone in Raman responses stimulated under 532 nm radiation. Lignin-like structures have been suggested to be present in fungi [50]. Furthermore, *Alternaria* group is known to exhibit active lignin biochemistry [51]. In this contribution we used the results of our theoretical studies on a lignin-like structural segment reported previously [26].

Density Functional Theory studies

To discuss Raman responses we conducted quantum chemical calculations using density functional theory (DFT) for the selected model systems using the 6-31++g(d,p) basis set and the restricted b3lyp functional [52] within the Gaussian 09 program package [53]. Resonant Raman spectra were computed using cphf=rdfreq option by Gaussian for the wavelength at 532 nm, as we used in experiment. The Raman intensities of the normal modes were calculated for the optimized structures. We used a scaling factor of 0.97 to map DFT frequencies in the spectral range of interest. To plot Raman spectral dispersions according to DFT predictions, we took convolutions with Lorentzian line-shape with full width at half maximum of 8 cm^{-1}.

To address optical electronic properties of the characteristic chromophores we took advantage of recent progress in time-dependent DFT (TD-DFT). Here, it is important to notice that while TD-DFT allows a straightforward study of excited states, typically, results lack ambiguity for transitions between the highest occupied molecular orbital and lowest unoccupied molecular orbital in simple molecular systems only. In other instances, computed optical transitions report substantial lists of involved orbitals without a single dominant component. To avoid this, we applied Koopmans theorem [54]: and to provide representations of electronic redistributions upon optical excitations in the visible spectral range, we transformed the computed transition density matrix [55] to represent the "particle" and 'hole" orbital components involved in the optical electronic transitions. Pairs of such orbital components constitute so-called natural transition orbitals (NTO) [56]. By visualizing NTOs of the electronic transitions responsible for optical density in the visible spectral range we provide a rigorous, up to the level of theory used, description of the electronic components that govern spectral responses in the visible spectral range. To plot optical electronic spectral dispersions according to TD-DFT predictions, we took convolutions with Lorentzian line-shape with full width at half maximum of 50 cm^{-1}. We provide an example of the information obtained using this approach in the main text, Fig. 4, with similar data for all molecules investigated being presented in the Supplementary Information.

RESULTS

Rapid growth of filaments on paper was confirmed under 100% humidity consistent with the results of previous studies [32]. Yeast growth of *Alternaria* group mainly was stimulated on paper soaked in water. We observed the opportunistic growth of several different fungal groups, such as *Alternaria*,

Chaetomium and *Aspergillus niger*, among which *Alternaria sp.* demonstrated a competitive dominance for experiments performed over a week. Specifically, in **Fig. 2A** and **2B** we present millimetre scale images of semi-dry and wet yeast colonial developments of *Alternaria sp.* on the paper surface. We present microscopy resolved filaments from the yeast in **Fig. 2C** and **2D**. **Figs. 2E-2H** show *Alternaria* sp. filament growth in paper (100% humidity) where the red marks indicate sites where Raman signals were taken. **Fig. 2I(J)** and **2K(L)** show different resolution images of initial colonial developments and conidia of the other species present, namely *Chaetomium* and *Aspergillus niger* group species, respectively. The liquid droplets at the surface of the filaments are the extra-enzymatic excretion of the filaments. In the case of *Chaetomium* group species, the rainbow-coloured regions (see **Fig. 2J**) are due to Fresnel interferences at the surface of enzymatic digestive excretions. Here, it is important to stress that the observed microstructures demonstrate dark colorations. This suggests the presence of various chromophores and depositions of pigments with electronic resonances in the ultraviolet-visible spectral range. Specifically, in **Fig. 2M** we show optical absorption spectra of methanol extracts of the three groups of organisms grown on paper. The spectra are complex and cannot be used for characterization of historical artefacts with organisms *in vivo*. In contrast, as resonant Raman microscopy is sensitive to molecular structure sampled microscopically and *in vivo*, we may use the technique to distinguish the spatial changes in chemical composition of different growing filaments.

In **Fig. 3A-F** we present the **main experimental** results of the study – Raman spectra taken at different spots of colonial growth of the *Alternaria sp.* group. Specifically, **Fig. 3A** demonstrates Raman spectra detected at the surface of a very wet yeast colony (as shown in **Fig. 2A** and **2B**). For reference, **Fig. 3B** compares the Raman response of a wet paper spot located several millimetres away from the yeast colony with the response characteristic of the office paper prior to fungal growth. While not the focus of the report, here it is important to note that fungal growth correlates with relative reduction of Raman intensities at 1086 and 1602 cm^{-1}. In a recent study, these peaks were discussed as spectral signatures of the COC β-glycosidic bond of cellulose and of lignin, respectively [57]. The observed changes may be considered consistent with the described enzymatic activities of fungi [6-10]. The presence of lignin components we discuss in the following section of the manuscript.

Next, **Fig. 3C** presents a response of a dry region (next to the yeast), where hyphae are starting to develop as shown in **Fig. 2C** and **2D**. To showcase the diversity of Raman signatures of the *Alternaria sp.* group, in **Fig. 3D-3F** we present Raman spectra sampled at the sites, as indicated by the red marks in **Fig. 2F-2H**, respectively, on dry hyphal filaments of *Alternaria sp.* Overall, the obvious variances of microscopically resolved Raman spectra (shown in **Fig. 3**) suggest structural and biochemical diversity, which one may anticipate to be according to rapid growth and expansion.

DISCUSSION

Electronic properties of model molecular systems

To approach molecular analysis using Raman micro-spectroscopy, first, we must explore the electronic properties of relevant model chromophores (see **Fig. 1**). This is necessary since we must account for the effect of excitation wavelength upon computations of pre-resonant Raman intensities. At the same time, after Raman assisted molecular analysis, the computed electronic spectra are valuable to review experimental data as shown in **Fig. 2M**. Therefore, in **Fig. 4**, we present the results of TD-DFT studies – optical electronic spectra of the considered molecular systems sorted according to the low energy edges of their optical absorption.

Our quantum chemistry studies predict that the chromophores of the first group, such as alternariol, flavosperone, funalenone and fonsecin would demonstrate optical absorption in the UV spectral range to provide yellow-brown coloration. Specifically, the optical absorption of alternariol [35] is according

to transitions at 316 and 244 nm suggesting a pale yellowish color: see second spectrum from the top in **Fig. 4A**. The corresponding first and seventh NTO pairs (see **Fig. 4 bottom**) demonstrate that in both cases the departure (particle) states are of bonding character, and the electron states demonstrate antibonding contributions. The hole state of the fourth pair shows a larger electronic delocalization for the third (non-methylated) ring. In the case of flavosperone, which was reported in a previous study as a yellow benzochromene or naphthopyran [36], theory predicts an optical absorption edge similar to that of alternariol, save the transition due to the first NTO pair at 377 nm is weaker. In **Fig. 4** we present the first and the second NTO pairs (to connect the bonding and anti-bonding molecular electronic components) which determine the optical absorption at 377 and 332 nm, respectively, as shown in **Fig. 4A**. Computed frequencies of the two transitions and their relative intensities are in reasonable agreement with previous experimental studies on this molecule [29]. Fonsecin naphtho-γ-pyrone metabolite [36] is the last chromophore we consider in this group. TD-DFT anticipates it to demonstrate the lower frequency edge of electronic optical absorptions with the first and second transitions at 396nm and 320 nm providing a yellow-orange color: see **Fig. 4**, this is consistent with previous studies for pigments extracted from *Alternaria* group organisms [58].

According to the results of TD-DFT studies, the second quinone-based chromophores demonstrate a very broad distribution of colors. In particular, the two computed optical transitions at 386 nm (NTO1) and 264nm (NTO5) of flavoglaucin confirm the reported yellow coloration of the hydroquinones [27,38]. On the other hand, erythroglaucin as has been isolated from *Aspergillus* and *Chaetomium* [28], as well as from *Alternaria* species [59] is reported as an orange-red colorant [60]. Indeed, our theory studies suggest strong optical density for the molecule at 480 nm (see the corresponding spectrum in **Fig. 4B** and NTO1 pair, in Supplementary information **Fig. S2**). Further, cycloleucomelon(e) green pigment [40] is anticipated to show a weak optical absorption at 685 nm (NTO1) and a more intense transition at 503 nm described by the second NTO pair (see Supplementary information **Fig. S2**).

Next, we explore electronic properties of two dimeric naphthopyrans (the third group of chromophores): both are structurally simplified: see the replacements of the methyl side groups with hydrogen atoms as indicated in **Fig. 1**. The main attention is placed on aurasperone: though originally isolated from *Aspergillus niger* [36], the metabolite has also been reported for *Alternaria* group species [58]. TD-DFT anticipates an optical absorption edge for this chromophore mainly driven by the second transition at 395 nm, while the first one at 413 nm (it is peculiar at it involves both aromatic systems) is expected to show a very weak intensity. In the case of isonigerone, theory predicts the optical absorption edge to be slightly more red: even though its first transition is more energetic NTO1 (402 nm), and comparing to that of aurasperone, it has a strong intensity: see Supplementary information **Fig. S3**. Considering the results of previous experimental studies of the optical electronic dispersions for aurasperone chromophores, our computation results are in excellent agreement [36,58].

Riboflavin (the fourth pteridine group) plays an important role in cellular respiration in various organisms with its electronic and vibration properties being extensively studied by both experimental and theoretical approaches [61,62]. Here, the computed energy and nature of the electronic redistribution (NTO pair 1) characteristic to the $S_0 \rightarrow S_1$ optical transition agrees well with results reported previously [61]. In our studies, however, we provide a description for the next intense optical electronic transition at 328 nm due to NTO pair 4: see **Fig. 4B** and Supplementary information **Fig. S4**. The outcome allows computing a suitable quality pre-resonance Raman spectrum for the molecule for the excitation wavelength at 530 nm (see **Fig. 3H**), necessary to discuss experimental spectra, see the following section of the manuscript.

As we have mentioned in the introduction, according to previous studies, chromophores of the fifth group do not play role in the *Alternaria* group. Instead, melanin pigments [27] and "green aspergilline" hexahydroxyl pentacyclic quinoid [28,29] are considered as maturity signatures of *Aspergilline niger* conidia. Nonetheless, since the chromophores are of an historical and general scientific value, here we characterize their optical electronic and Raman properties. To describe the former molecular system, we used a eumelanin-melanin trimer with structure as shown in **Fig. 1**. The selected structure resembles the trimer as explored previously [47] but includes three dihydroxyindole carboxylic acids, with the third terminating the chain without favourable intramolecular hydrogen bonding. As a result, the wavelength of the $S_0 \rightarrow S_1$ optical transition is blue shifted (see **Fig. 4B** and Supplementary information **Fig. S5**) compared to the results reported for the optimal eumelanin-melanin trimer, while the character of electronic redistribution upon the optical transition is comparable to that in the optimal system [46]. At the same time, the computed electronic edge is consistent with that reported for melanin extracts from *Aspergillus niger* [63] and agrees with the optical spectrum we detect as reported in **Fig. 2M**. Such agreement, however, should not be taken as evidence that the structure of the selected eumelanin-melanin trimer is characteristic of the material in nature. The structural diversity of melanin biopolymers *in vivo* is very large. Our selection is simply a possible motif. Using the computed electronic properties, we calculate pre-resonance Raman for this system (**see Fig. 3H**) which reproduces quite well the main resonances reported in the literature [64]: for details see Supplementary information **Fig. S5**. In the case of hexahydroxyl pentacyclic quinoid, theory predicts a pair of near infrared optical electronic transitions: see NTO1 and NTO2 pairs specific to electronic transitions at 767 and 713 nm, respectively. Hence, we may search for an explanation of the green color of the chromophore, as reported in literature [28,29], if we consider the third optical transition at 458 nm: see the corresponding NTO3 pair in Supplementary Information **Fig. S5**.

Carotenoids have extended π-electron conjugated chains, which stimulate research considering their possible role in redox reactions [65,66]. The calculated optical absorption of asperyellone and β-carotene are in general consistent with results reported for such systems in literature [66,67]. At the same time, our computed NTO presentations for the electronic transitions in the two systems provide a more systematic perspective in visualization of the electronic redistributions involved in the computed optical transitions: see Supplementary Information **Fig. S6**. One may clearly see that the frequency of the first (lowest energy) resonance for asperyellone at 462 nm is blue shifted compared to β-carotene (at 569 m,) which is due to the lesser extent of its π-electron conjugation. Further the NTO presentation allows a systematic description of the electronic transitions in relation to optical absorption, an approach that is a challenge using molecular orbitals [66].

Raman responses of the model systems

Accounting for the electronic properties of the model chromophores we are ready to explore predictions of their Raman responses: see **Fig. 3G** and **3H**. For systems where transitions are distant from the stimulation wavelength comparable intensities and relative intensities of peaks of non-resonant (grey) and resonant (red) Raman responses (e.g. alternariol and funalenone) are observed, **Fig. 3G**. For systems where the stimulation wavelength is close to the wavelength of an electronic transition then there are differences in intensities and relative intensities of peaks of the calculated non-resonant (grey) and resonant (red) Raman spectra (e.g. asperyellone), **Fig. 3H**. Further, for such systems we scale the resonant contributions (e.g. fonsecin, funalenone, cycloleucomelon(e) and beta-carotene). The sensitivity of Raman to the excitation wavelength is expected: resonances involve electronic to electron-vibrational coupling with the pre-resonant Raman intensity of each normal mode being related to its Raman tensor and an electronic transition dipole moment [23-25]. Further, as such relations are specific to structure, we should make predictions of Raman responses using quantum chemistry according to the experimental conditions used.

Interpretation and spectral assignments

To facilitate assignments, in **Fig. 5**, we group and annotate the computed responses of the most promising model systems to address the experimental spectra shown in **Fig. 3C** and **3E**. Specifically, considering the results of our DFT studies, we simplify the molecular analysis (according to the experimentally derived Raman data) by both: a) comparing computed responses of chromophores that have electronic resonances far from the excitation wavelength with the experimental spectra, we ignore molecules whose responses do not match the patterns of observed resonance even if the computed spectral signatures are scaled to match the intensities of resonantly enhanced responses (10-1000 times); b) we give preference to the computed signals in molecular systems where we expect the largest Raman intensity under resonant excitation, as used in experiment. Descriptions of all Raman modes, regardless of whether they are present in our samples are provided in the Supplementary Information for use in analysis of other colored organisms.

According to the first criterion, we should not expect alternariol, funalenone and flavosperone (see their spectra in **Fig. 3G**) to contribute to the detected Raman response. The chromophores should be present, but our experimental setting would not allow their detection. Next, we consider the response of the model glycopeptide, considered as a structural-constituent component of filaments. Indeed, the computed spectrum (see **Fig. 3G** and **5A**) fits the results of recent coherent Raman studies on yeast cells and spores of *Schizosaccharomyces pombe* [48]. However, such a Raman contribution if present would be in the background of the resonant Raman responses as shown in **Figs. 3A-F**. Overall, this sorting is consistent with the observation that the studied microstructures demonstrate dark colorations suggesting the presence of various chromophores with electronic resonances in the ultraviolet-visible spectral range. Therefore, in the analysis described below we follow the second criterion to understand the likely chromophores present.

According to **Fig. 3H**, the melanin group of chromophores is expected to provide strong pre-resonance Raman. Such molecular forms are known in respect to maturation of *Aspergillius* fungi, mainly [28-29]. For our analysis of *Alternaria* Sp. we do not observe any comparable resonances in our experimental data as theory computes, so contributions of eumelanin-melanin and hexahydroxyl pentacyclic quinoid to the overall Raman response is unlikely.

We now consider molecules where strong pre-resonant enhancement may be expected. Let us first consider the intense Raman peaks at 1150 and 1509 cm^{-1} (**Fig. 3A**) detected at the site of yeast growth, as shown in **Fig. 2A**, to specific modes (144 and 216) computed for β-carotene: see the Supplementary Information file. Theory also predicts the pattern of smaller peaks: see **Fig. 3H**. Our assignments are consistent with previous definitions [68] and we note that β-carotene has been reported as a product of *Alternaria alternata* [35]. Interestingly, β-carotene Raman signatures are not observed in the filaments (**Fig. 3C**), which initiate within and from yeast depositions. These filament cells are at the very surface of paper or buried in the paper interface: see **Fig. 2C, D**. Nonetheless, the older hyphae microstructures - filaments which grow above the surface, do demonstrate a pair of intense resonances: see the star marked peaks in **Fig. 5B**. These resonances are typical for carotenes, but shifted to lower frequencies. Since a dependence of Raman response on the conjugation length of carotenes has been reported [69], we may suggest that the older filaments, which protrude away from the paper surface, may contain pigments which show more extensive conjugation than β-carotene and not yet identified analytically.

Next, if we compare the Raman spectra of the filaments at the surface (**Fig. 3C**) and the mature hyphae filaments above (**Fig. 3D-F**) we see that the former is rich with numerous relatively narrow resonances, save the contributions of paper, which we may distinguish according to the spectrum annotated in **Fig. 5A**. The rich set of Raman peaks indicates a complex molecular content and, therefore rich biochemistry during early growth. The observed pattern of narrow peaks in the 1200 - 1400 cm^{-1} suggests the presence of flavoglaucin. At the same time the relatively weak Raman resonances above

1600 cm^{-1} may suggest contributions of riboflavin and cycloleucomelon(e), which are expected in early filaments. Information on the normal modes of these chromophores are provided in the Supporting Information File. Of course, here, we should notice a good agreement of the computed Raman activities (**Fig. 5A**) of a lignin-like structure as shown in **Fig. 1**. The contribution of lignin in Raman responses sampled at fungi on paper was described previously [57] and was discussed as critically important for *Alternaria* sp. biology [51]. Indeed, comparing our experimental and theoretical studies [26], a lignin-like component is likely to contribute into Raman activities at 1606 and 1700 cm^{-1}. In Supplementary information **Fig. S21** we show that in our lignin model systems the normal modes at about 1600 cm^{-1} involve admixture of C-C stretching and CCH bending localize on aromatic rings, while the activities at 1700 cm^{-1} are specific to carbonyls.

We now consider the older mature filament structures (**Fig. 5B**) that function to provide a three-dimensional scaffold and transport pathway to support feeding of the colony. Accounting for the line-shapes in **Fig. 3D-F**, we can rule out contributions of flavoglaucin, riboflavin, cycloleucomelon(e) and asperyellone to the signals taken from the mature filaments. Here, we do not observe the computed lignin-like structure spectral feature at 1700 cm^{-1} that accompanies Raman activity at 1606 cm^{-1} as for the experimental data presented in **Fig. 5A** which may be due to naturally present structural diversity of lignin *in vivo*. Also, since there is an absence of sharp dominant resonances at about 1300 and 1350 cm^{-1}, we rule out the contribution of isonigerone. Taking these considerations into account we ascribe the main broad pre-resonant Raman responses as shown in **Fig. 3D-F** as likely arising from fonsecin, erythroglaucin and aurasperone. Such chromophores have been extracted from *Alternaria group* species [41,58]. We should also consider contributions of lignin-like structural components, as well [57]. Finally, here, as we have already mentioned, the two narrow intense resonances (star marks in **Fig. 5B**) may be ascribed to carotenoids, which exhibit more extensive conjugation than β-carotene.

Accounting for the electronic properties of model chromophores anticipated in various fungi [27-46], we compute pre-resonance Raman spectra to assign experimental Raman responses sampled under microscopic resolution in dependence on conditions of fungal growth on paper. Using the assignments, we may review the optical absorption spectrum detected in methanol extracts from *Alternaria sp*. growing on paper: see **Fig. 2M**. Accordingly, we may ascribe the visible absorption band at 520 nm to erythroglaucin and carotene electronic resonances, while fonsecin, aurasperone and lignin would contribute to the UV optical absorption edge at 400 nm. In result, we demonstrate that if assisted with quantum chemistry, Raman microscopy is a helpful tool for the characterization of in vivo fungal growth, biochemistry and physiology in dependence on environment and structure.

CONCLUSIONS

We use resonant Raman microscopy to explore the spatial diversity of chromophores in fungal conidia and hyphae stimulated to grow on standard office paper in humid/ wet conditions. Though we observe growth of *Alternaria*, *Chaetomium* and *Aspergillus* group species on paper, here we focus on the Raman responses for *Alternaria* structures, which dominated growth under the chosen conditions and have been little studied spectroscopically. To identify the molecular characteristics of the species present we use quantum chemistry to calculate the spectral response of a range of chromophores representative of families of fungal metabolites with optical absorption in the ultraviolet-visible spectral range. For some of the molecular systems this is for the first time.

We show that β-carotene dominates in yeast depositions at the paper surface and fonsecin, erythroglaucin and aurasperone type chromophores dominate in mature hyphae. Further, resonance Raman of mature hyphal filaments suggests a spectral contribution of carotenes longer than β-carotene. Resonant Raman spectral data from specific parts of developing hyphae indicate a complex biochemistry with the presence of lignin, flavoglaucin, riboflavin, cycloleucomelon(e) and

asperyellone type molecular components in filaments initiating within and from yeast depositions. The data presented suggests a rich biochemistry is required to stimulate development of a mature three-dimensional scaffold. We show that when assisted with quantum chemistry, Raman assisted molecular analysis supports the review of optical electronic responses under microscopy resolution. The described approach is a promising tool for the characterization of fungal growth, biochemistry, and physiology in dependence on environment and structure. In the Heritage field, the experimental approach and the library of optical and structural data are useful for the study of the effect of fungi on a wide range of objects made from paper including books, prints, drawings, watercolors, engravings and even sculptures [5,7,13-17,31].

DECLARATION OF CONFLICT OF INTEREST

The authors declare no conflict of interest.

ACKNOWLEDGEMENTS

The authors acknowledge funding from the NTU Global Heritage: Science, Management & Development, Seed-Corn/Mid-Career Research Fund 2019-2020 and AFOSR FA9550-1-20-0206. Rajeharish Rajendran is thanked for collection of Raman spectra of papers presented in the Supporting Information.

REFERENCES

1. Bengtson S, Rasmussen B, Ivarsson M, Muhling J, Broman C, Marone F, Stampanoni M, Bekker A. Fungus-like mycelial fossils in 2.4-billion-year-old vesicular basalt. Nature Ecology & Evolution 2017;1:0141. https://doi.org/10.1038/s41559-017-0141.

2. Wehmer C. On the production of citric acid by fermentation. Amer Mic Soc Proc 1893;15:90.

3. Whittaker RH. New concepts of kingdoms of organisms. Science 1969;163:150-161. https://doi.org/10.1126/science.163.3863.150.

4. Roman C, Diaconescu R, Scripcariu L, Grigoriu A. Biocides used in preservation, restoration and conservation of the paper. Eur J Sci Theol 2013;9:263-271.

5. Michaelsen A, Pinar G, Pinzari F. Molecular and microscopical investigation of the microflora inhabiting a deteriorated Italian manuscript dated from the thirteenth century. Microb Ecol 2010;60:69–80. http://dx.doi.org/10.1007/s00248-010-9667-9.

6. Falih AM. Production of extracellular enzymes by some soil yeasts. Qatar Univ Sci J 1997;17:97-102.

7. Pinzari F, Zotti M, De Mico A, Calvini P. Biodegradation of inorganic components in paper documents: Formation of calcium oxalate crystals as a consequence of Aspergillus terreus Thom growth. Int Biodet & Biodegr 2010;64:499-505. https://doi.org/10.1016/j.ibiod.2010.06.001.

8. Ohkuma M, Maeda Y, Johjima T, Kudo T. Lignin degradation and roles of white rot fungi: Study on an efficient symbiotic system in fungus-growing termites and its application to bioremediation. Riken Review. 2001;39-42.

9. Dennis C. Breakdown of cellulose by yeast species. J Gen Microbiol 1972;71:409-411. https://doi.org/10.1099/00221287-71-2-409.

10. Stevens B, Payne J. Cellulase and xylanase production by yeasts of the genus Trichosporon. J Gen Microbiol 1977;100:381-393. https://doi.org/10.1099/00221287-100-2-381.

11. Mills JS, White R. The organic chemistry of museum objects. 2nd ed. Oxford: Butterworth-Heinemann Ltd.; 1994.

12. Gallo F, Pasquariello G, Rocchetti F. Biological Investigation on Sizings for Permanent Papers. Restaurator 1998;19:61-84. https://doi.org/10.1515/rest.1998.19.2.61.

13. Melo D, Sequeira SO, Lopes JA, Macedo MF. Stains versus colourants produced by fungi colonising paper cultural heritage: A review. Journal of Cultural Heritage 2019;35:161-182. https://doi.org/10.1016/j.culher.2018.05.013.

14. Florian MLE. Fungal Facts - Solving Fungal Problems in Heritage Collections. Archetype Publications, Great Britain; 2002.

15. Zotti M, Ferroni A, Calvini P. Inhibition properties of simple fungistatic compounds on fungi isolated from foxing spots. Restaurator 2007;28:201-217. https://doi.org/10.1515/REST.2007.201.
16. Szczepanowska H, Lovett CM. A study of the removal and prevention of fungal stains on paper. J Am Inst Conserv 1992;31:147-160. https://doi.org/10.1179/019713692806066664.
17. Rebrikova NL, Manturovskaya NV. Foxing: A new approach to an old problem. Restaurator 2000;21:85-100. https://doi.org/10.1515/REST.2000.85.
18. Peters D. An alternative to foxing? Oxidative digradation as a cause of cellulosic discolouration. Papier Retaurierung 2000;1:Suppl55-60.
19. Bicchieri M, Pappalardo G, Romano FP, Sementilli FM, De Acutis R. Characterization of foxing stains by chemical and spectrometric methods. Restaurator 2001;22:1-19. https://doi.org/10.1515/REST.2001.1.
20. Tang LC. Determination of iron and copper in 18th and 19th century books by nameless atomic absorption spectroscopy. Journal of the American Institute for Conservation 1978;17:19-32.
21. Iiams TM, Beckwith TD. Note on the causes and prevention of foxing on books. The Library Quarterly 1935;5:407-418.
22. Hey M. Foxing: Some unanswered questions. The Antiquarian Book Monthly Review 1983;113;340-343.
23. Placzek G. Rayleigh and Raman Scattering. UCRL Trans. No.526 L. Handbuch der Radiologie. E. Marx, Leipzig, Akademische Verlagsgesellechaft; 1934;2:209-374.
24. Albrecht AC. On the Theory of Raman Intensities. J Chem Phys 1961;34:1476-1484. https://doi.org/10.1063/1.1701032.
25. Spiro TG, Strekas TC. Resonance Raman Spectra of Hemoglobin and Cytochrome c: Inverse Polarization and Vibronic Scattering. Proc Nat Acad Sci 1972;69:2622-2626. https://doi.org/10.1073/pnas.69.9.2622.
26. Volkov VV, Hickman GJ, Sola-Rabada A, Perry CC. Distributions of Silica and Biopolymer Structural Components in the Spore Elater of *Equisetum arvense*, an Ancient Silicifying Plant Frontiers in Plant Science 2019;10:210. https://doi.org/10.3389/fpls.2019.00210.
27. Wolf FA. Synthesis of Various Products, Especially Pigments, by Fungi. Journal of the Elisha Mitchell Scientific Society 1973;89:184-205.
28. Ray AC, Eakin RE. Studies on the biosynthesis of aspergillin by Aspergillus niger. Appl Microbiol 1975;30:909-915.
29. Nielsen KF, Mogensen JM, Johansen M, Larsen TO, Frisvad JC. Review of secondary metabolites and mycotoxins from the Aspergillus niger group. Anal Bioanal Chem 2009;395:1225-1242. https://doi.org/10.1007/s00216-009-3081-5.
30. Tyc KM, Kühn C, Wilson D, Klipp E. Assessing the advantage of morphological changes in Candida albicans: a game theoretical study. Frontiers in Microbiology 2014;5:41. https://doi.org/10.3389/fmicb.2014.00041.
31. Koestler RJ, Koestler VR, Charola AE, Nieto-Fernandez FE. Art, biology, and conservation: biodegradation of works of art. The Metropolitan Museum of Art, New York 2003. ISBN: 1-56639-107-8.
32. Pinzari F, Pasquariello G, De Mico A. Biodeterioration of Paper: A SEM Study of Fungal Spoilage Reproduced Under Controlled Conditions. Macromolecular Symposia 2006;238:57-66. https://doi.org/10.1002/masy.200650609.
33. Macedo F. Fungi in archives, libraries, and museums: a review on paper conservation and human health. Critical Reviews in Microbiology 2019;45:686-700. https://doi.org/10.1080/1040841X.2019.1690420.
34. Agarwal UP, Reiner RS, Ralph SA. Cellulose I crystallinity determination using FT–Raman spectroscopy: univariate and multivariate methods. Cellulose 2010;17:721–733.
35. Haggblom P, Unestam T. Blue Light Inhibits Mycotoxin Production and Increases Total Lipids and Pigmentation in Alternaria alternata. Appl Environ Microbiol 1979;38:1074-1077. https://doi.org/10.1128/AEM.38.6.1074-1077.1979.

36. Tanaka H, Wamg PL, Yamada O, Tamura LT. Yellow Pigments of Aspergillus niger and Asp. awamori. Part I. Isolation of Aurasperone A and Related Pigments. Agr Biol Chem 1966;30:107-113. https://doi.org/10.1080/00021369.1966.10858561.
37. Inokoshi J, Shiomi K, Masuma R, Tanaka H, Yamada H, Omura S. Funalenone, a novel collagenase inhibitor produced by *Aspergillus niger*. The Journal of Antibiotics 1999;52:1095-1100. https://doi.org/10.7164/antibiotics.52.1095.
38. Quilico A, Panizzi L, Mugnaini E. Structure of Flavoglaucin and Auroglaucin. Nature 1949;164:26-27. https://doi.org/10.1038/164026a0.
39. Gould BG, Raistrick H. Studies in the biochemistry of micro-organisms: The crystalline pigments of species in the Aspergillus glaucus series. Biochemical Journal 1934;28:1640-1858. https://doi.org/10.1042/bj0281640.
40. Quilico A, Panizzi L. Chemische Untersuchungen über Aspergillus echinulatus, I. Mitteilung. Berichte der deutschen chemischen Gesellschaft 1943;76:348-358. https://doi.org/10.1002/cber.19430760408.
41. Dufossé L, Fouillaud M, Caro Y, Mapari S, Sutthiwong N. Filamentous fungi are large-scale producers of pigments and colorants for the food industry. Cur Opin Biotech 2014;26:56-61. https://doi.org/10.1016/j.copbio.2013.09.007.
42. Buckingham J. Dictionary of Natural Products, Chapman&Hall; 1994;1:A00001-C02529:1226. ISBN 10:0412466201.
43. Hiort J, Maksimenka K, Reichert M, Perović-Ottstadt S, Lin WH, Wray V, Steube K, Schaumann K, Weber H, Proksch P, Ebel R, Müller WEG, Bringmann G. New natural products from the sponge-derived fungus Aspergillus niger. J Nat Prod 2004;67:1532-1543. https://doi.org/10.1021/np030551d.
44. Wang S, Li XM, Teuscher F, Li DL, Diesel A, Ebel R, Proksch P, Wang BG. Chaetopyranin, a benzaldehyde derivative, and other related metabolites from Chaetomium globosum, an endophytic fungus derived from the marine red alga Polysiphonia urceolata. J Nat Prod 2006;69:1622-1625. https://doi.org/10.1021/np060248n.
45. S. Lu, J. Yian, W. Sun, J. Meng, X. Wang, X. Fu, A. Wang, D. La, Y. Liu, L. Zhou. Bis-naphtho-gammapyrones from fungi and their bioactivities. Molecules 2014;19:7169-7188.
46. Huang HB, Feng XJ, Liu L, Chen B, Lu YJ, Ma L, She ZG, Lin YC. Three dimeric naphtho-γ-pyrones from the mangrove endophytic fungus Aspergillus tubingensis isolated from Pongamia pinnata. Planta Med 2010;76:1888-1891. https://doi.org/10.1055/s-0030-1249955.
47. Marchetti B, Karsili TNV. Theoretical insights into the photo-protective mechanisms of natural biological sunscreens: building blocks of eumelanin and pheomelanin. Phys Chem Chem Phys 2016;18:3644-3658. https://doi.org/10.1039/C5CP06767G.
48. Noothalapati H, Sasaki T, Kaino T, Kawamukai M, Ando M, Hamaguchi H, Yamamoto T. Label-free Chemical Imaging of Fungal Spore Walls by Raman Microscopy and Multivariate Curve Resolution Analysis. Scientific Reports 2016;6:27789. https://doi.org/10.1038/srep27789.
49. Couturier M, et al., Lytic xylan oxidases from wood-decay fungi unlock biomass degradation. Nature Chemical Biology 2018;14:306-310. https://doi.org/10.1038/nchembio.2558.
50. Thom C, Phillips M. Lignin-like complexes in fungi. Journal of the Washington Academy of Sciences 1932;22:237-239.
51. Sharma A, Aggarwal NK, Yadav A. First Report of Lignin Peroxidase Production from Alternaria alternata ANF238 Isolated from Rotten Wood Sample, Bioengineering and Bioscience 2016;4:76-87.
52. Becke AD. Density functional exchange energy approximation with correct asymptotic behaviour. Phys Rev A 1988;38:3098. https://doi.org/10.1103/PhysRevA.38.3098.
53. Frisch MJ, Trucks GW, Schlegel HB, Scuseria GE, Robb MA, Cheeseman JR, et al. Gaussian 09, revision B.01. Wallingford CT: Gaussian Inc.; 2010.
54. Koopmans T. Über die Zuordnung von Wellenfunktionen und Eigenwerten zu den einzelnen Elektronen eines Atoms. Physica 1934;1:104-113.
55. Amos AT, Hall GG. Single determinant wave functions. Proc Royal Soc A 1961;263:483-493. https://doi.org/10.1098/rspa.1961.0175.

56. Martin RL. Natural transition orbitals. J Chem Phys 2003;118:4775-4777. https://doi.org/10.1063/1.1558471.
57. Chiriu D, Ricci PC, Cappellini G, Salis M, Loddo G, Carbonaro CM. Ageing of ancient paper: A kinetic model of cellulose degradation from Raman spectra. Journal of Raman Spectroscopy 2018;49:1802-1811. https://doi.org/10.1002/jrs.5462.
58. Shaaban M, Shaaban KA, Abdel-Aziz MS. Seven naphtho-γ-pyrones from the marine-derived fungus Alternaria alternata: structure elucidation and biological properties. Org Med Chem Lett 2012;2:6. https://doi.org/10.1186/2191-2858-2-6.
59. Suemitsu R, Iwai J, Kawaguchi K, Haitani N, Kitagawa N. Isolation and Identification of Erythroglaucin (1, 4, 5-Trihydroxy-7-methoxy-2-methylanthraquinone) from the Mycelium of Alternaria porri (Ellis) Ciferri. Agricultural and Biological Chemistry 1977;41:2289-2290. https://doi.org/10.1080/00021369.1977.10862849.
60. Caro Y, Venkatachalam M, Lebeau J, Fouillaud M, Dufossé L. Pigments and Colorants from Filamentous Fungi. Fungal Metabolites. Springer 2017;1-70.
61. Klaumünzer B, Kröner D, Saalfrank P. (TD-)DFT calculation of vibrational and vibronic spectra of riboflavin in solution. J Phys Chem B 2010;114:10826-10834. https://doi.org/10.1021/jp100642c.
62. Yun MJ, Cheong BS, Cho HG. Surface-enhanced Raman Spectroscopy and Density Functional Theory Studies of Riboflavin, Lumiflavin, and Lumichrome Adsorbed on Silver Colloids. Bull. Kor Chem Soc 2019;40:1183-1190. https://doi.org/10.1002/bkcs.11898.
63. Capozzi V, Perna G, Carmone P, Gallone A, Lastella M, Mezzenga E, Quartucci G, Ambrico M, Augelli V, Biagi PF, Ligonzo T,Minafra A, Schiavulli L, Pallara M, Cicero R. Optical and photoelectronic properties of melanin. Thin Solid Films 2006;511-512:362-366. https://doi.org/10.1016/j.tsf.2005.12.065.
64. V. Capozzi, G. Perna, A. Gallone, P. F. Biagi, P. Carmone, A. Fratello, G. Guida, P. Zanna, R. Cicero. Raman and optical spectroscopy of eumelanin films. J Mol Struct 2005;744-747:717-721. https://doi.org/10.1016/j.molstruc.2004.11.074.
65. Galinato MG, Niedzwiedzki D, Deal C, Birge RR, Frank HA. Cation radicals of xanthophylls. Photosynth Res 2007;94:67-78. https://doi.org/10.1007/s11120-007-9218-5.
66. Ghosh D, Hachmann J, Yanai T, Chan GKL. Orbital optimization in the density matrix renormalization group, with applications to polyenes and -carotene. J Chem Phys 2008;128:144117. https://doi.org/10.1063/1.2883976.
67. Llansola-Portoles MJ, Pascal AA, Robert B. Electronic and vibrational properties of carotenoids: from in vitro to in vivo. J R Soc Interface 2017;14:20170504. https://doi.org/10.1098/rsif.2017.0504.
68. Tschirner N, Schenderlein M, Brose K, Schlodder E, Mroginski MA, Thomsena C, Hildebrandt P. Resonance Raman spectra of β-carotene in solution and in photosystems revisited: an experimental and theoretical study. Phys Chem Chem Phys 2009;11:11471-11478. https://doi.org/10.1039/B917341B.
69. Withnall R, Chowdhry BZ, Silver J, Edwards HGM, de Oliveira LFC. Raman spectra of carotenoids in natural products. Spectrochimica Acta Part A: Molecular and Biomolecular Spectroscopy 2003;59:2207-2212. https://doi.org/10.1016/s1386-1425(03)00064-7.

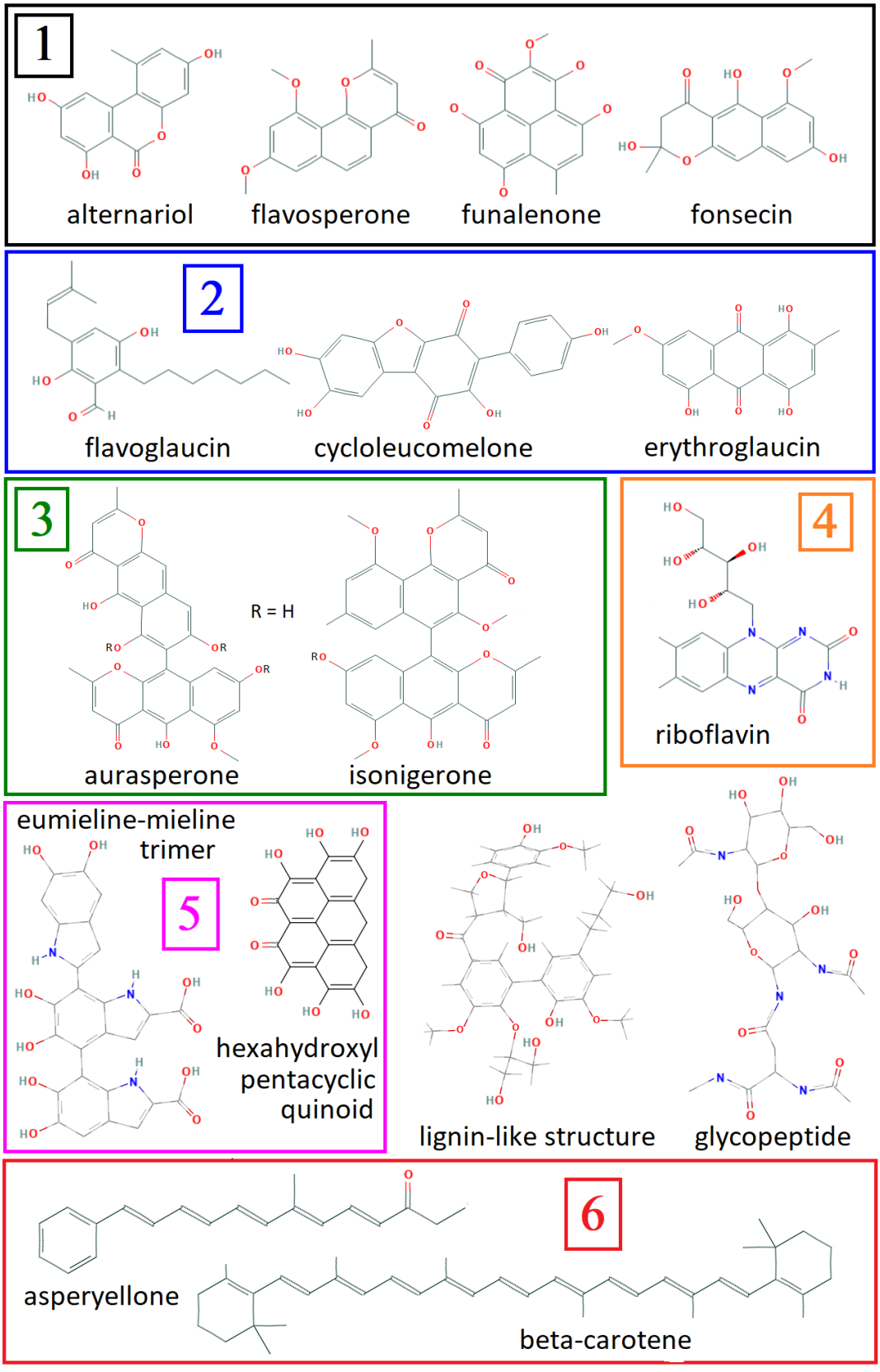

Fig. 1. Chemical structures of the chromophores studied by computation.

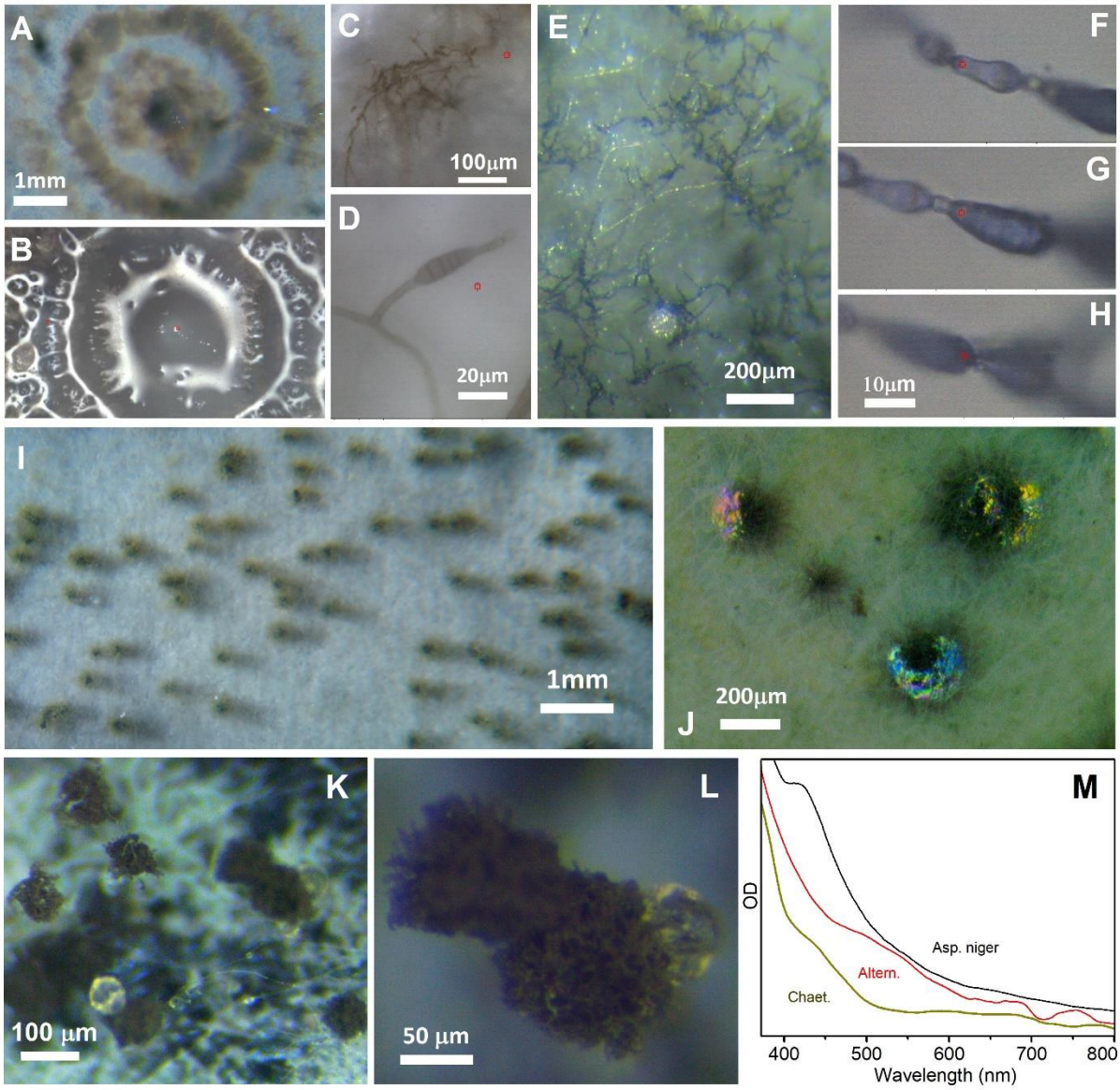

Fig. 2. Microscopy resolved images of opportunistic fungal growth on paper stimulated under different wetting and humidity conditions. A-D: yeast growth (mainly *Alternaria* sp.) stimulated in wet paper. E-H: *Alternaria* sp. filament growth in paper under 100% humidity: red marks indicate sites where Raman signals were taken. I-J: microscopy images of colonial expansion of *Chaetomium* sp. K-L: microscopy images of hyphae and conidia of *Aspergillus niger* (group). M: optical absorption spectra of pigments and chromophore in methanol extracts of the three groups of organisms grown on paper as indicated.

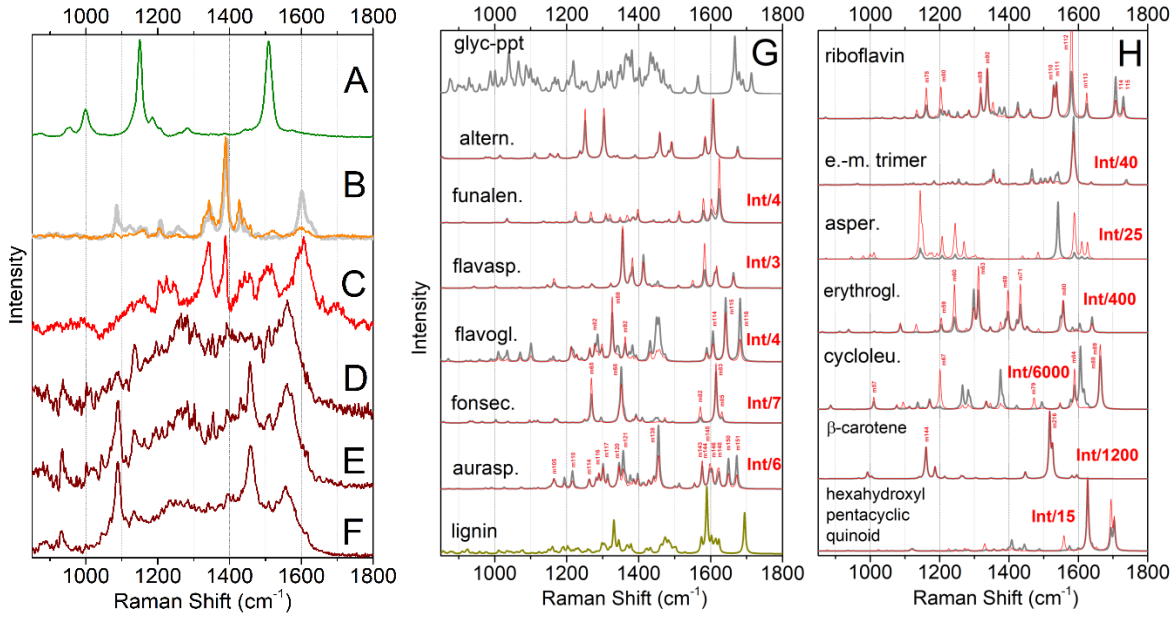

Fig. 3. Experimental Raman data collected from fungal structures (*Alternaria* sp.) using radiation at 532 nm and computed spectra of selected chromophores. A: responses detected at colonial sites as shown in **Fig. 2B**. B: Raman spectra of new office paper (gray) and of wet paper millimetres away from a yeast growth site (orange) as shown in **Fig. 2A and 2B**. C: Raman responses of *Alternaria* sp. filaments growing from yeast depositions in contact with the surface or cavitating in the paper surface: as shown in **Fig. 2C-2E**. D-F: Raman responses of *Alternaria* sp. hyphae growing well above the paper substrate at sites as indicated by red marks in **Fig. 2F-2H**. G, H: computed resonant (red) and non-resonant (grey) Raman spectra of a range of chromophores. Indices list the normal modes described in **SI Fig. S7 – Fig. S20**.

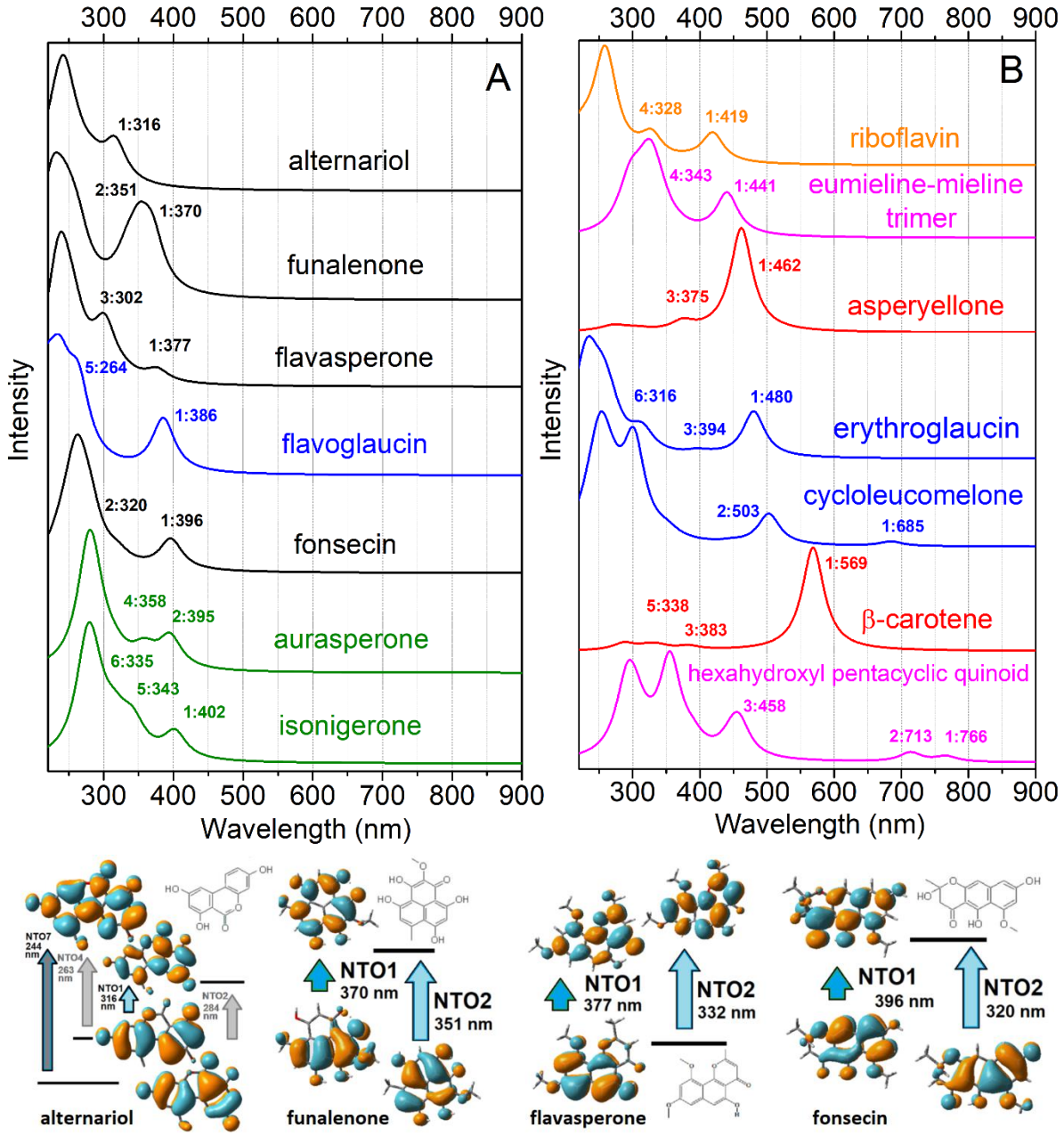

Fig. 4. Computed optical electronic spectra for representative chromophores of the first (black), second (blue), third (green), fourth (orange), fifth (magenta) and sixth (red) group arranged according to their edge absorption. NTO and resonances for chromophores of the first chromophore group, alternariol, funalenone, flavosperone and fonsecin: descriptions for other chromophores are in the Supporting information file

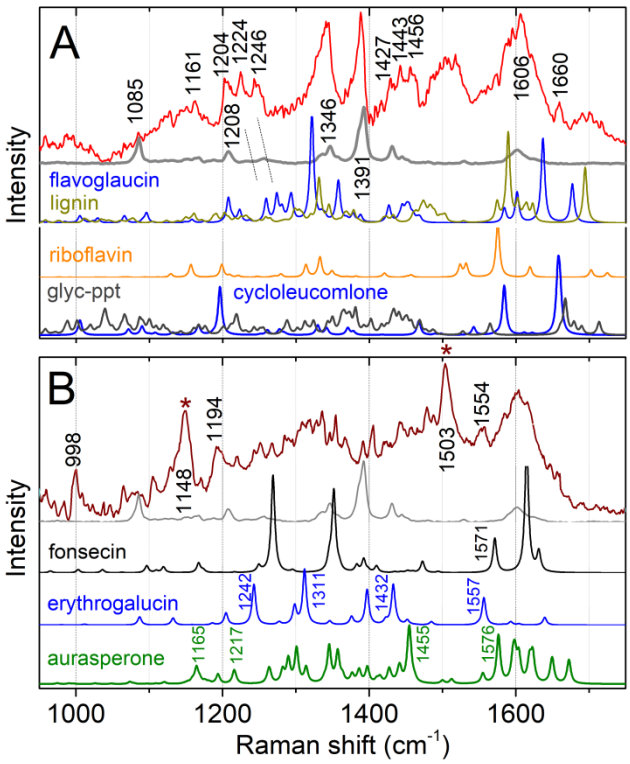

Fig. 5. Comparison of experimental Raman responses of filaments growing from yeast depositions in contact with the surface or cavitating in the paper surface. A: annotated experimental spectrum of living tissue growing from yeast filaments (red line) as in **Fig. 3C** and experimental response of paper (grey line) compared with the computed responses of flavoglaucin, lignin, riboflavin and glycopeptide, as indicated. B: annotated experimental spectrum of mature filaments (wine line) as in **Fig. 3E** and experimental response of paper (grey line) compared with the computed responses of fonsecin, erythroglaucin, aurasperone as indicated. Asterisks, next to the experimental peaks at 1150 and 1509 cm^{-1}, indicate resonances which correspond to Raman activities typical for carotenes [26,69], also see the spectrum computed for β-carotene, as shown in **Fig. 3H**. However, their slightly lower frequencies suggest more extensive conjugation than in β-carotene [68].